CDF note 10173

Measurement of Top Quark and Anti-top quark mass difference in the Lepton+jets channel

The CDF Collaboration
URL http://www-cdf.fnal.gov
(Dated: June 7, 2010)

We report a measurement of the mass difference between top quark and anti-top quark (ΔM_{top}) in the Lepton+Jets channel using $p\bar{p}$ collisions at $\sqrt{s} = 1.96$ TeV from 5.6 fb^{-1} of data collected with the CDF detector at the Fermilab Tevatron. A top quark mass difference (Δm_{reco}) is reconstructed for every event by minimizing a χ^2-like function to the overconstrained kinematics of the $t\bar{t}$ system with assumption of averaged top quark mass (M_{top}) equal to 172.5 GeV/c^2. To use more information of mass difference, we include a reconstructed mass difference from 2^{nd} best χ^2 fit ($\Delta m^{(2)}_{reco}$). The values of Δm_{reco} and $\Delta m^{(2)}_{reco}$ for 2294 Lepton+Jets candidate events including both zero b-tagging and b-tagged events are compared to two-dimensional probability density function derived by applying kernel density estimation to fully simulated MC events with different values of the mass difference in the detector. We measure $\Delta M_{top} = -3.3 \pm 1.4$ (stat.) $\pm$ 1.0 (syst.) GeV/c^2.

Preliminary Results of ΔM_{top} *using* 5.6 *fb* $^{-1}$

I. INTRODUCTION

This note describes a measurement of the mass difference of top quark and anti-top quark (ΔM_{top}) from $t\bar{t}$ events using $p\bar{p}$ collisions at $\sqrt{s} = 1.96$ TeV with the CDF detector at the Tevatron. The mass of the top quark is very precisely measured to be 173.1 ± 1.3 [1]. Therefore it is straight forward to test that top quark has same mass with anti-top quark which is unique place to test mass difference of the quark and anti-quark [2]. The mass of particle should be same with the mass of its anti-particle under the CPT theorem. However CPT can be violate in principle if some of new physics from non-local theory is involved [3]. The test of CPT violation have been done in many sector. However it was not well done in quark sector and high energy regime as like top quark. The recent measurement from D0 collaboration was done using 1 fb^{-1} of data and had a consistent result with standard model (SM) [4].

Top quarks are produced predominantly in pairs at the Tevatron, and in the SM decay nearly 100% of the time to a W boson and a b quark. The topology of a $t\bar{t}$ event is determined by the decay of the two W bosons, as each W boson can decay to a lepton-neutrino pair ($l\nu$) or to a pair of quarks (qq'). We look for events consistent with $t\bar{t}$ production and decay involving one $l\nu$ pair (we do not consider events with taus) and another qq' pair which we call lepton+jets channel. The CDF detector is described in Ref. [5].

Our measurement is a template-based measurement, meaning that we compare quantities in data with distributions from simulated MC events to find the mass difference. To reconstruct events with our hypothesis, we modify kinematic fitter of top quark mass reconstruction that have been used in top quark mass measurement [6–8] using knowledge of the overconstrained kinematics of the $t\bar{t}$ system. In this kinematic fitter, we allow mass difference as described in Section III to reconstruct mass difference ($\Delta m_{\rm reco}$).

We choose minimum χ^2 case between different jets-to-partons assignments to reconstruct $\Delta m_{\rm reco}$. In addition, we use 2^{nd} observable from 2^{nd} minimum χ^2 combination ($\Delta m^{(2)}_{\rm reco}$) to increase statistical power.

Monte Carlo samples generated with MADGRAPH [9] generator for 17 different ΔM_{top} from -20 GeV/c^2 to 20 GeV/c^2 and parton-showered with PYTHIA [10] are run through a full CDF detector simulation. The values of observables in data are compared to each point in the MC grid using a non-parametric approach based on Kernel Density Estimation (KDE) [11]. Local Polynomial Smoothing [12] is used to smooth out these points and calculate the probability densities at any arbitrary value of ΔM_{top}. An unbinned likelihood fit is used to measure ΔM_{top}. All of these technique already well proved by top quark mass measurement [6, 13].

II. EVENT SELECTION

At the trigger level, Lepton+Jets candidate events are selected by requiring a high-E_T electron (or high-p_T muon). In addition, large $\not\!\!E_T$ + two jets requirement is used to increase muon acceptance. Offline, the events are required to have a single energetic lepton (electron or muon), large $\not\!\!E_T$ due to the escaping neutrino from the leptonic W decay, and at least four jets in the final state. Electron candidates are identified as a high-momentum track in the tracking system matched to an electromagnetic cluster reconstructed in the calorimeters with $E_T > 20$ GeV. We also require that energy shared by the towers surrounding the cluster is low. Muon candidates are reconstructed as high-momentum tracks with $p_T > 20$ GeV/c matching hits in the muon chambers. Energy deposited in the calorimeter is required to be consistent with a minimum ionizing particle. The $\not\!\!E_T$ is required to be greater tham 20 GeV. To further rejection of QCD multijet background contribution, we require $H_T > 250$ GeV/c and QCD veto cut, which is rejection of events having very close (less than 0.5) leading jet with $\not\!\!E_T$ in ϕ angle for $\not\!\!E_T < 30$ GeV/c^2 events.

Jets are reconstructed with the JETCLU [14] cone algorithm using a cone radius of $R \equiv \sqrt{\eta^2 + \phi^2} = 0.4$. To improve the statistical power of the method, samples are divided into subsamples, depending on the number of jets identified as b quarks using SECVTX [15] algorithm and lepton charge. In the exactly zero tag and one tag events, we require exactly four jets with $E_T > 20$ GeV/c^2. For the event with more than one tag, which have more statistical power and less background, we loosen these cuts, and allow events with more than four jets. We also loosen the cut on the 4th jet to $E_T > 12$ GeV/c^2 to increase the number of such events.

We make a cut on the χ^2 out of the kinematic fitter, requiring it to be less than 3.0 for 0 tag events and 9.0 for 1 and more than 1 tag events. Finally, in order to properly normalize our probability density functions, we define hard boundaries on the values of the observables. Events with values of an observable falling outside the boundary are rejected. Event selection is summarized in Tables I.

TABLE I: Event selection and observed numbers of events for the two Lepton+Jets event categories

	0-tag	1-tag	2-tag
b-tags	==0	==1	>1
Leading 3 jets E_T(GeV/c^2)	>20	>20	>20
MET (GeV/c^2)	>20	>20	>20
H_T (GeV/c)	>250	>250	>250
4th jet E_T(GeV/c^2)	>20	>20	>12
Extra jets E_T(GeV/c^2)	<20	<20	Any
χ^2	<3	<9	<9
$\Delta m_{\rm reco}$ boundary cut (GeV/c^2)	$-200<\Delta m_{\rm reco}<200$	$-200<\Delta m_{\rm reco}<200$	$-200<m_t^{\rm reco}<200$
$\Delta m^{(2)}_{\rm reco}$ boundary cut (GeV/c^2)	$-200<\Delta m^{(2)}_{\rm reco}<200$	$-200<\Delta m^{(2)}_{\rm reco}<200$	$-200<m_t^{\rm reco(2)}<200$

III. EVENT RECONSTRUCTION

The value of the reconstructed mass difference ($\Delta m_{\rm reco}$) is determined by minimizing a χ^2 describing the overconstrained kinematics of the $t\bar{t}$ system. The reconstructed mass difference is a number that distills all the kinematic information in each event into one variable that is a good estimator for the true mass difference (ΔM$_{\rm top}$). The kinematic fitter uses knowledge of the lepton and jet four-vectors, b-tagging information and the measured $\not\!\!E_T$. The invariant masses of the lepton-neutrino pair and the dijet mass from the hadronic W decay are constrained to be near the well-known W mass. We assumed that averaged top quark mass is 172.5 GeV/c^2 and then, allow leptonic and hadronic top quark mass deviated by $dM_{reco}/2$ from 172.5 GeV/c^2.

$$\begin{aligned}\chi^2 &= \Sigma_{i=\ell,4jets}\frac{(p_T^{i,fit}-p_T^{i,meas})^2}{\sigma_i^2}+\Sigma_{j=x,y}\frac{(U_j^{fit}-U_j^{meas})^2}{\sigma_j^2}\\ &+ \frac{(M_{jj}-M_W)^2}{\Gamma_W^2}+\frac{(M_{\ell\nu}-M_W)^2}{\Gamma_W^2}\\ &+ \frac{(M_{bjj}-(172.5+dM_{reco}/2))^2}{\Gamma_t^2}+\frac{(M_{b\ell\nu}-(172.5-dM_{reco}/2))^2}{\Gamma_t^2}\end{aligned} \quad \text{(III.1)}$$

is minimized for every jet-parton assignment consistent with b-tagging. The first sum constrains the p_T of the jets and lepton, within their uncertainties, to remain close to their measured values. The second term constrains the unclustered energy in the event to remain near its measured value, providing a handle on the neutrino 4-vector. The W boson has a small width, and the two W mass terms provide the most powerful constraints in the fit. The last two terms in the χ^2 constrain the three-body invariant masses of each top decay chain to have mass difference between top quark and anti-top quark. The reconstructed mass difference ($\Delta m_{\rm reco}$), which is corresponding to top quark mass minus anti-top quark mass in reconstruction level, can be calculated as below,

$$\Delta m_{\rm reco} = -Q_{lepton}\times dM_{reco} \quad \text{(III.2)}$$

The single jet-parton assignment with the lowest χ^2 that is consistent with b-tagging gives the value of $\Delta m_{\rm reco}$ for the event. Events where the lowest $\chi^2>3.0$ (or 9.0) are rejected for zero b-tagged (or b-tagged) events.

Although $\Delta m_{\rm reco}$ carry a lot of information about ΔM$_{\rm top}$, it is still possible to choose wrong combination from minimum χ^2 which means that we can have ΔM$_{\rm top}$ information from another combination of jet-parton assignment. We add another reconstructed mass difference from the 2^{nd} smallest χ^2 combination which is $\Delta m^{(2)}_{\rm reco}$. We use this value as 2^{rd} observable.

Due to difference response of leptonic and hadronic top, $\Delta m_{\rm reco}$ distributions are very different between positive and negative lepton events. To increase statistical power of measurement, we divide our samples using lepton charge.

IV. BACKGROUNDS

An *a priori* estimate for the Lepton+Jets background composition is used to derive background shapes for $\Delta m_{\rm reco}$, and $\Delta m^{(2)}_{\rm reco}$. ALPGEN [16] combined with PYTHIA showering is used to model W+jets. Contributions include W$b\bar{b}$, W$c\bar{c}$, Wc and W+light flavor (LF) jets. QCD background is modeled by releasing a few of lepton identification cut (anti-electron). The relative fractions of the different W+jets samples are determined in MC, but the absolute

TABLE II: Expected number of background and signal events after event selection.

CDF II Preliminary 5.6 fb^{-1}

	0-tag(+)	0-tag(-)	1-tag (+)	1-tag(-)	2-tag(+)	2-tag(-)
W$b\bar{b}$	16.1±5.2	18.6±6.0	15.0±4.9	16.5±5.3	3.9±1.3	4.2±1.4
W$c\bar{c}$	51.5±15.3	58.3±16.8	9.3±3.0	10.6±3.3	0.6±0.2	0.6±0.3
Wc	24.2±8.5	25.3±8.8	4.6±1.8	4.8±1.9	0.4±0.2	0.4±0.2
W+LF	191.8±39.0	210.5±38.4	13.1±3.0	14.4±3.1	0.5±0.1	0.5±0.1
Z+jets	24.5±5.0	24.3±4.4	2.9±0.7	2.8±0.6	0.4±0.1	0.4±0.1
single top	2.0±0.2	2.0±0.2	2.9±0.3	2.6±0.2	1.2±0.1	1.0±0.1
Diboson	26.7±2.5	23.4±2.2	3.4±0.4	3.2±0.4	0.4±0.1	0.6±0.1
QCD	47.3±37.8	48.5±36.6	7.1±5.7	7.6±6.4	1.5±1.7	0.9±1.5
Total	384.0±61.9	408.5±62.0	58.4±11.7	62.6±12.6	8.8±2.4	8.5±2.4
$t\bar{t}$	210.9±28.3	214.7±29.1	287.6±35.9	290.4±36.5	139.0±13.8	142.6±14.2
Observed	645	633	340	380	142	154

normalization is derived from the data. The MC are combined using their relative cross sections and acceptances, and we remove events overlapping in phase space and flavor across different samples. MC and theoretical cross-sections are used to model the single-top and diboson backgrounds. The expected number of background from different sources is shown in Table II. More detail of background modeling can be found in Ref. [17].

V. KERNEL DENSITY ESTIMATES

Probability density functions for $\Delta m_{\rm reco}$-$\Delta m^{(2)}_{\rm reco}$ at every point in the $\Delta {\rm M_{top}}$ grid and for backgrounds are derived using a Kernel Density Estimate (KDE) approach [11]. KDE is a non-parametric method for forming density estimates that can easily be generalized to more than one dimension, making it useful for this analysis, which has two observables per event. The probability for an event with observable (x) is given by the linear sum of contributions from all entries in the MC:

$$\hat{f}(x) = \frac{1}{nh}\sum_{i=1}^{n} K(\frac{x-x_i}{h}). \tag{V.1}$$

In the above equation, $\hat{f}(x)$ is the probability to observe x given some MC sample with known $\Delta {\rm M_{top}}$. The MC has n entries, with observables x_i. The kernel function K is a normalized function that adds less probability to a measurement at x as its distance from x_i increases. The smoothing parameter h (sometimes called the bandwidth) is a number that determines the width of the kernel. Larger values of h smooth out the contribution to the density estimate and give more weight at x farther from x_i. Smaller values of h provide less bias to the density estimate, but are more sensitive to statistical fluctuations. We use the Epanechnikov kernel, defined as:

$$K(t) = \frac{3}{4}(1-t^2) \text{ for } |t| < 1 \text{ and } K(t) = 0 \text{ otherwise,} \tag{V.2}$$

so that only events with $|x - x_i| < h$ contribute to $\hat{f}(x)$. We use an adaptive KDE method in which the value of h is replaced by h_i in that the amount of smoothing around x_i depends on the value of $\hat{f}(x_i)$. In the peak of the distributions, where statistics are high, we use small values of h_i to capture as much shape information as possible. In the tails of the distribution, where there are few events and the density estimates are sensitive to statistical fluctuations, a larger value of h_i is used. The overall scale of h is set by the number of entries in the MC sample (larger smoothing is used when fewer events are available), and by the RMS of the distribution (larger smoothing is used for wider distributions). We extend KDE to two dimensions by multiplying the two kernels together:

$$\hat{f}(x,y) = \frac{1}{n}\sum_{i=1}^{n} \frac{1}{h_{x,i}h_{y,i}}\left[K(\frac{x-x_i}{h_{x,i}}) \times K(\frac{y-y_i}{h_{y,i}})\right]. \tag{V.3}$$

Figure 1 show the 2d density estimates for signal events ($\Delta {\rm M_{top}} = 0$ GeV/c^2). Figures 2 show the 2d estimates of background events. To estimate the background density, we combined each background sample with the appropriate weights taking into account the sample size and cross section, and then had KDE estimation.

VI. LIKELIHOOD FIT

The values of $\Delta m_{\rm reco}$-$\Delta m^{(2)}_{\rm reco}$ observed in data are compared to points in $\Delta {\rm M}_{\rm top}$ space. An extended maximum likelihood fit is performed to maximize the likelihood with respect to the expected number of signal (n_s) and background events (n_b) in each of the six subsamples. A Gaussian constraint on the expected number of background events is applied to each of the subsamples. The likelihood for subsample k with N events is given by:

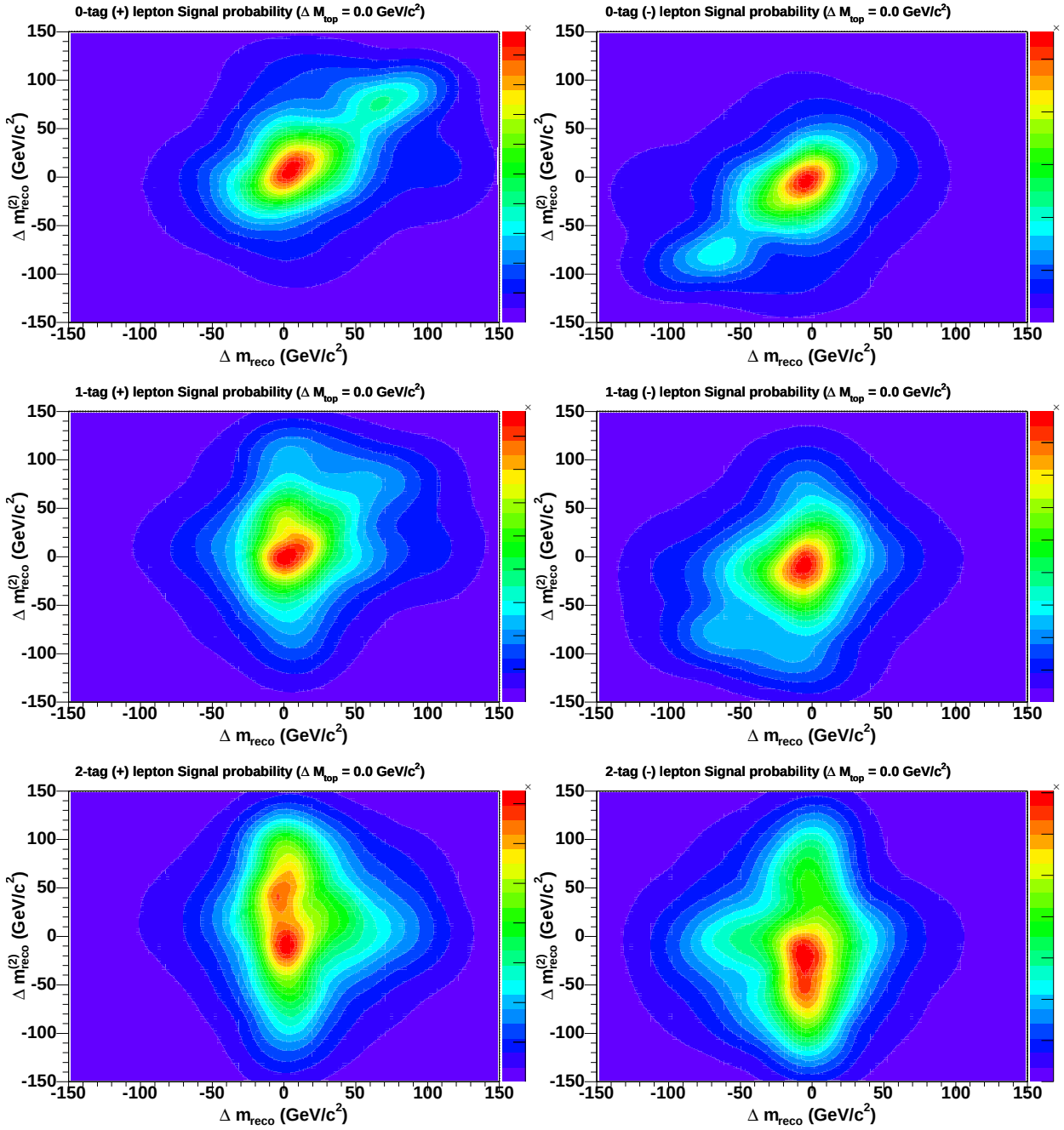

FIG. 1: 2d density estimates for input $\Delta {\rm M}_{\rm top} = 0.0$ GeV/c^2 signal

$$\mathcal{L}_k = \exp\left(-\frac{(n_b - n_b^0)^2}{2\sigma_{n_b}^2}\right) \times \prod_{i=1}^{N} \frac{n_s P_{sig}(\Delta m_{\rm reco}, \Delta m^{(2)}_{\rm reco}; \Delta {\rm M_{top}}) + n_b P_{bg}(\Delta m_{\rm reco}, \Delta m^{(2)}_{\rm reco})}{n_s + n_b}. \quad \text{(VI.1)}$$

The overall likelihood is a product over the six individual subsample likelihoods:

$$\mathcal{L} = \mathcal{L}_{\text{0-tag, (+) lepton}} \times \mathcal{L}_{\text{0-tag, (-) lepton}} \times \mathcal{L}_{\text{1-tag, (+) lepton}} \times \mathcal{L}_{\text{1-tag, (-) lepton}} \times \mathcal{L}_{\text{2-tag, (+) lepton}} \times \mathcal{L}_{\text{2-tag, (-) lepton}}. \quad \text{(VI.2)}$$

The above gives values of $-\ln \mathcal{L}$ only for points in the $\Delta {\rm M_{top}}$ grid corresponding to generated MC points, and not as

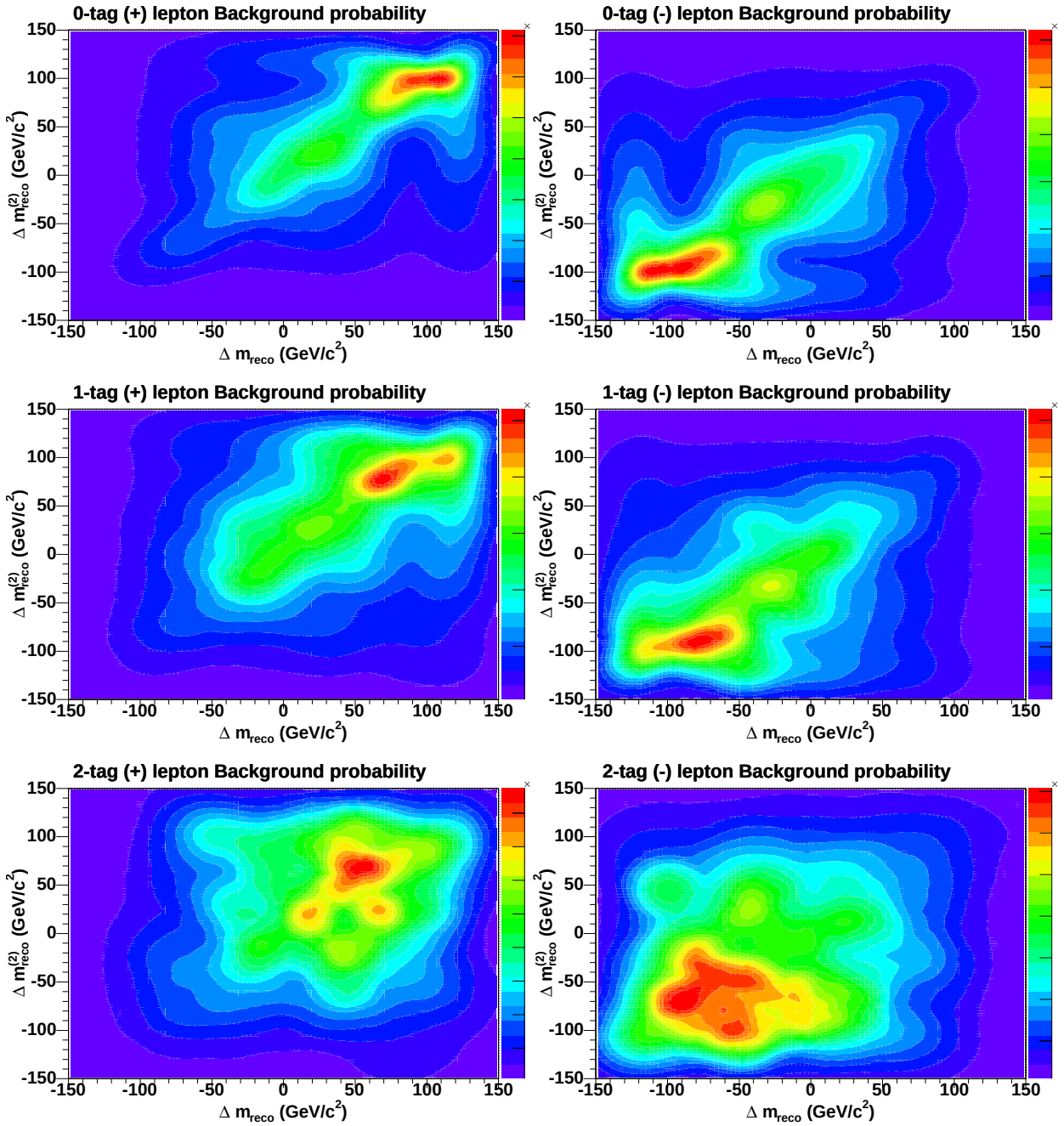

FIG. 2: 2d density estimates for backgrounds

a continuous function. To obtain density estimates for an arbitrary point in the ΔM_{top} grid, we use local polynomial smoothing [12] on a per-event basis. This allows for a smooth likelihood that can be minimized. The measured uncertainty on ΔM_{top} comes from the largest possible shift in ΔM_{top} on the $\Delta \ln \mathcal{L} = 0.5$.

VII. METHOD CHECK

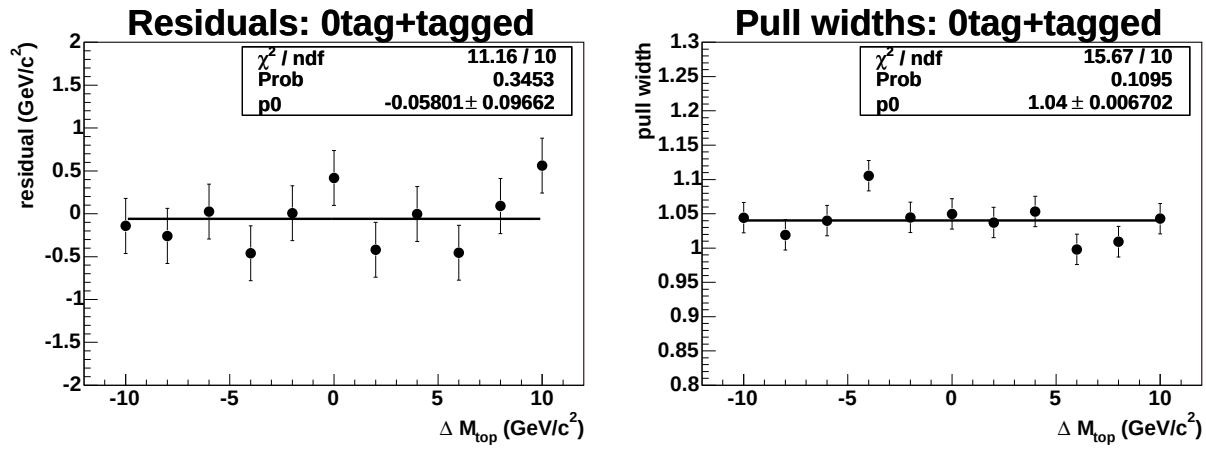

FIG. 3: Residual shift of mass difference (left) and pull widths (right) as a function of input ΔM_{top} from pseudoexperiments.

We test our machinery by running pseudoexperiments with varying values of ΔM_{top} from -10 GeV/c^2 to 10 GeV/c^2. Figure 3 (left) shows the ΔM_{top} residuals as a function of true ΔM_{top}. We can see that there is no bias on our measurement. Right plot shows pull width of our measurement. We need to increase our measured uncertainty by 4.0% which is applied to all of systematic studies and data fits.

VIII. RESULTS

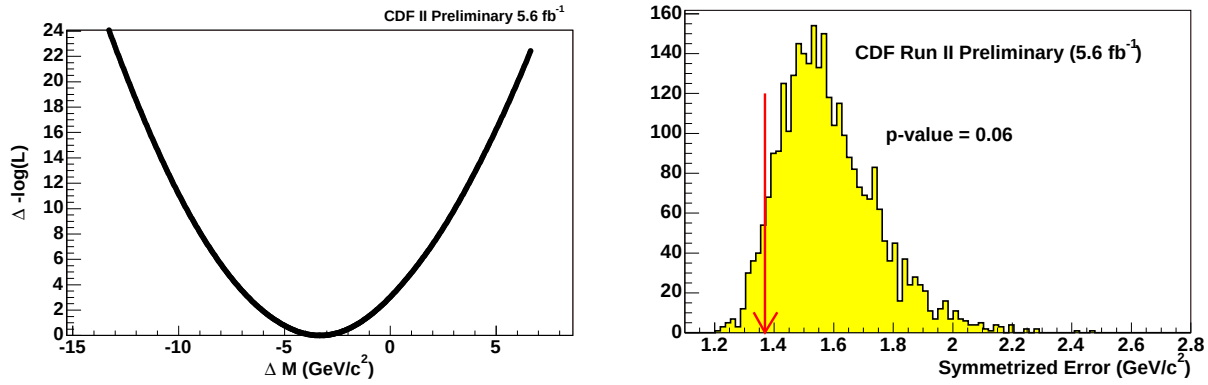

FIG. 4: (Left) Negative log-likelihood of data fit. (Right) P-value plot of measured uncertainty with expectation from pseudo-experiments.

The likelihood procedure when applied to the data yields $\Delta M_{top} = -3.3 \pm 1.4$ GeV/c^2. The 1d Δlog-likelihood is shown in Figure 4 left. As shown in Figure 4 right, only 6% of pseudoexperiments have a smaller error than the value measured in data.

TABLE III: Summary of systematics. All numbers have units of GeV/c^2.

CDF II Preliminary 5.6 fb^{-1}

Systematic	Result (GeV/c^2)
Signal Modeling	0.7
JES	0.2
PDFs	0.1
b jet energy	0.1
$b/\bar{b}$ asymmetry	0.3
Background shape	0.2
gg fraction	0.1
Radiation	0.1
MC statistics	0.1
Lepton energy	0.1
MHI	0.4
Color Reconnection	0.2
Total systematic	1.0

IX. SYSTEMATIC UNCERTAINTIES

We examine a variety of effects that could systematically shift our measurement. Dominant systematic uncertainty is signal modeling. Comparing pseudoexperiments generated with MADGRAPH and PYTHIA gives an estimate of one part of the signal modeling. We also take different parton showering from HERWIG [18] compared with nominal PYTHIA parton showering as an another part of signal modeling. We apply variations within uncertainties of Jet Energy Scale (JES) calibrations [19] in both signal and background pseudodata and measure resulting shifts in ΔM_{top} from pseudoexperiments, giving a JES uncertainty. We also vary the energy of b jets, which have different fragmentation than light quarks jets, as well as semi-leptonic decays and different color flow, resulting in a b-JES systematic. Effects due to uncertain modeling of radiation including initial-state radiation (ISR) and final-state radiation (FSR) are studied by extrapolating uncertainties in the p_T of Drell-Yan events to the $t\bar{t}$ mass region, resulting in a radiation systematics. A systematic on different parton distribution functions is obtained by varying the independent eigenvector of the CTEQ6M set, comparing parton distribution functions with different values of Λ_{QCD}, and comparing CTEQ5L with MRST72. We also test the effect of reweighting MC to increase the fraction of $t\bar{t}$ events initiated by gg (vs qq) from the 6% in the leading order MC to 20%. Systematics due to lepton energy scales are estimated by propagating 1% shifts on electron and muon energies scales. Background composition systematics are obtained by varying the fraction of the different types of backgrounds in pseudoexperiments and the normalization of total backgrounds. We also vary the uncertain Q^2 of background events in a background shape systematic. It has been suggested that color reconnection effects could cause a bias in the top quark mass measurement [20]. We account Color Reconnection [20] systematics by generating MCs with and without CR and taking the difference as systematics. Because we are measuring mass difference, we investigate possible systematics from different response of b quark and $\bar{b}$ quark. We measure $p_T$balance of b and $\bar{b}$ quarks using dijet sample by SECVTX b-tagging both jets with identifying the flavor using soft muon of leptonic decay of b. We measured $p_T$balance difference between MC and data and propage to $b/\bar{b}$ asymmetry systematics. We also investigate the effect of faking lepton charge by 1% added in lepton $p_T$systematics.

The total systematic error is 1.0 GeV/c^2. The systematics are summarized in Table III.

X. CONCLUSIONS

We present a measurement of the mass difference between top quark and anti-top quark in the Lepton+Jets channel using a template-based technique. Using 2d templates derived from Kernel Density Estimation and 5.6 fb^{-1} of data collected by the Tevatron, we measure

$$\Delta M_{top} = -3.3 \pm 1.4 \text{ (stat.)} \pm 1.0 \text{ (syst.) GeV}/c^2 = -3.3 \pm 1.7 \text{ GeV}/c^2$$

Acknowledgments

We thank the Fermilab staff and the technical staffs of the participating institutions for their vital contributions. This work was supported by the U.S. Department of Energy and National Science Foundation; the Italian Istituto Nazionale di Fisica Nucleare; the Ministry of Education, Culture, Sports, Science and Technology of Japan; the Natural Sciences and Engineering Research Council of Canada; the National Science Council of the Republic of China; the Swiss National Science Foundation; the A.P. Sloan Foundation; the Bundesministerium für Bildung und Forschung, Germany; the Korean Science and Engineering Foundation and the Korean Research Foundation; the Science and Technology Facilities Council and the Royal Society, UK; the Institut National de Physique Nucleaire et Physique des Particules/CNRS; the Russian Foundation for Basic Research; the Ministerio de Ciencia e Innovación, and Programa Consolider-Ingenio 2010, Spain; the Slovak R&D Agency; and the Academy of Finland.

---

[1] CDF and D0 Collaborations, FERMILAB-TM-2427-E (2009), arXiv:0903.2503v1.
[2] J.A.R. Cembranos, A. Rajaraman, and F. Takayama, Europhys. Lett. **82** (2008) 21001.
[3] D. Colladay and V. A. Kostelecky, Phys. Rev. D **55** (1997) 6760; J. P. Hsu and M. Hongoh, Phys. Rev. D **6** (1972) 256; C. Ragiadakos and C. Zenses, Phys. Lett B **76** (1978); G. Barenboim and J. Lykken, Phys. Lett. B **554** (2003) 73; Y. A. Sitenko and K. Y. Rulik, Eur. Phys. J. C **28** (2003) 405; R. S. Raghavan, JCAP **0308** (2003) 002; H. Belich *et al.*, Phys. Rev. D **68** (2003) 065030.
[4] V. M. Abazov, *et al.*, Phys. Rev. Lett. **103**, 132001 (2009).
[5] F. Abe, *et al.*, Nucl. Instrum. Methods Phys. Res. A **271**, 387 (1988).
[6] T. Aaltonen, *el al.*, Phys. Rev. D **79**, 092005 (2009).
[7] A. Abulenci, *et al.*, Phys. Rev. D **73**, 032003 (2006).
[8] A. Abulenci *et al.*, Phys. Rev. Lett. **96**, 022004 (2006).
[9] J. Alwall, *et al.*, J. High Energy Phys. **0709**, 028 (2007).
[10] T. Sjostrand, S. Mrenna, and P. Skands, J. High Energy Phys. **0605**, 026 (2006).
[11] K. S. Cranmer, Comput. Phys. Commun. **136**, 198 (2001).
[12] C. Loader, *Local Regression and Likelihood*, New York, USA, (Springer, 1999).
[13] T. Aaltonen, *el al.*, Phys. Rev. D **81**, 031102 (2010).
[14] F. Abe, *et al.*, Phys. Rev. D **45**, 1448 (1992).
[15] T. Affolder, *et al.*, Phys. Rev. D **64**, 032002 (2001).
[16] M. L. Mangano, *et al.*, J. High Energy Phys. **0307**, 001 (2003).
[17] T. Aaltonen, *et al.*, arXiv:1004.3224v1 (2010).
[18] G. Corcella, *et al.*, J. High Energy Phys. **0101**, 010 (2001).
[19] A. Bhatti, *et al.*, Nucl. Instrum. Methods Phys. Res. A **566**, 375 (2006).
[20] P. Z. Skands, D. Wicke, Eur. Phys. J. C **52**, 133 (2007).